

Domain wall fermion zero modes on classical topological backgrounds

P. Chen, N. Christ, G. Fleming, A. Kaehler,
C. Malureanu, R. Mawhinney, C. Sui, P. Vranas and Y. Zhestkov

Columbia University
Physics Department
New York, NY 10027

August 25, 2018

Abstract

The domain wall approach to lattice fermions employs an additional dimension, in which gauge fields are merely replicated, to separate the chiral components of a Dirac fermion. It is known that in the limit of infinite separation in this new dimension, domain wall fermions have exact zero modes, even for gauge fields which are not smooth. We explore the effects of finite extent in the fifth dimension on the zero modes for both smooth and non-smooth topological configurations and find that a fifth dimension of around ten sites is sufficient to clearly show zero mode effects. This small value for the extent of the fifth dimension indicates the practical utility of this technique for numerical simulations of QCD.

1 Introduction

The anomalous breaking of the flavor singlet axial symmetry of QCD, $U_A(1)$, has important physical consequences. It is responsible for the relatively large mass of the η' [1], [2] and effects the order of the finite temperature phase transition [3]. A central role in this is played by the index theorem [4] which relates the winding of the gauge field with the number of zero modes of the Dirac operator.

On the lattice the winding of the gauge field can not be defined unambiguously and the index of a finite-dimensional lattice Dirac operator is necessarily zero. Therefore, strictly speaking, the index theorem is not valid on the lattice. However, an approximate form of this theorem may still be present and govern anomalous effects. Some time ago this issue was investigated in [5] for the case of staggered and Wilson fermions. A first step in that direction was to ask to what extent the lattice Dirac operator for staggered and Wilson fermions develops the appropriate number of zero modes for a fixed smooth gauge field background with given winding. It was found that for a particular background the appropriate number of zero modes was generated but they were not robust when high frequency noise was superimposed. Furthermore, the background chosen was of a very special nature and did not have the spatial variation present, for example, in an instanton-like background. Recent work [6], with more realistic instanton-like backgrounds, has demonstrated that staggered fermions do not develop zero modes unless the lattice spacing, a , becomes very small ($a/D \ll 0.1$, where D is the instanton diameter). These difficulties suggest that for QCD, staggered fermions may fail to reproduce anomalous effects unless the lattice spacing is made quite small—considerably smaller than that used in present QCD thermodynamics studies, performed with $N_T \leq 8$ and staggered fermions.

Current numerical results for the order of the finite temperature phase transition for two flavor QCD with light quarks show that it is not first order [7]. This is consistent with the analysis in [3], provided $U_A(1)$ is broken. However, current lattice discretizations manifestly break the symmetry of the classical action at finite lattice spacing and the corresponding discretized Dirac operators have difficulty seeing zero modes for non-smooth topological configurations. This raises the possibility that the present apparent second-order character of the two-flavor QCD phase transition may be a result of lattice artifacts rather than physical, anomalous symmetry breaking. A recent explicit calculation of an anomalous difference of susceptibilities near the two-flavor QCD phase transition, using a spectral sum-rule sensitive to zero modes, showed effects at or below the 15% level [8]. However, in other work [9], suggestions of anomalous zero-mode effects were seen. Clearly, a lattice fermion formulation whose action has the full global symmetry content of the continuum theory at finite lattice spacing would be a very useful tool for studying anomalous symmetry breaking effects.

2 Domain Wall Fermions

A novel approach with spectacular zero mode properties has been developed during the past few years. Domain Wall Fermions were first introduced in [10] and a variant suitable for vector gauge theories was introduced in [11], [12], [13]. (For reviews see [14] and references

therein.) In this approach an extra space time dimension (henceforth to be called “ s ”) is introduced with free boundary conditions on the two four-dimensional boundaries, $s = 0$ and $s = L_s - 1$, where L_s is the extent of this new fifth dimension in lattice units. The fermion fields are defined in this extended space-time but the gauge fields are still defined on the ordinary space time and have no s dependence and no s component [15]. In this sense, the extra direction can be thought of as a sophisticated “flavor” space. Along the s direction the fermion field develops surface modes that are exponentially bound to the two free boundaries (domain walls) with the plus chirality component of the Dirac spinor on one boundary and the minus chirality on the other. As the size in lattice spacings (L_s) of this direction is increased the two chiral components get separated with only an exponentially small overlap remaining. For finite L_s this overlap breaks chiral symmetry by an exponentially small amount and as L_s tends to infinity chiral symmetry is restored. Therefore, L_s provides a new parameter that can be used to control the regularization induced chiral symmetry breaking at *any* lattice spacing. For the first time the approach to the chiral limit has been separated from the approach to the continuum limit.

An appealing aspect of the domain wall fermion formulation is the fact that the chirally symmetric, $L_s \rightarrow \infty$ limit can be analyzed in some detail using the overlap formalism [15]. Central to this overlap method are two Fock space states, designated $|0_H\rangle$ and $|0'\rangle$ in the notation of [12], constructed from four-dimensional, single-particle, fermionic states. Because the gauge field is independent of s , it is possible to develop an s -independent transfer matrix (T) and associated Hamiltonian along this direction. Now in the $L_s \rightarrow \infty$ limit, T^{L_s} becomes a projection operator onto the vacuum state, defined as $|0_H\rangle$, the Fock-space state in which all the negative energy states of H are filled. The second state $|0'\rangle$ is a much simpler, kinematic construction in which all single-particle eigenstates of position and γ^5 , with negative γ^5 eigenvalue, are filled.

A fermion Green’s function for a given gauge field background can then be expressed as a simple matrix element of the appropriate number of creation and annihilation operators inserted between the states $|0'\rangle$ and $|0_H\rangle$. In particular, the five-dimensional fermion determinant in the massless case is simply proportional to $|\langle 0'|0_H\rangle|^2$ which, for a finite space-time volume, can be calculated explicitly numerically. If the number of filled levels in $|0_H\rangle$ and $|0'\rangle$ is the same then $|\langle 0'|0_H\rangle|^2 \neq 0$. However, if these filling levels differ, then $|\langle 0'|0_H\rangle|^2 = 0$ for zero mass and finite volume. This implies the presence of exact zero modes in the five-dimensional formulation. For a Green’s function to be non-zero, an appropriate number of creation and annihilation operators must be inserted to balance the deficit. The deficit is naturally integer-valued and is defined as the index of the lattice Dirac operator. Therefore, this method provides a way to associate an index with the lattice fermion operator in the limit $L_s \rightarrow \infty$ but at fixed lattice spacing [15].

More specifically it was found [15], [16] that for classical backgrounds these zero modes are exact, that the deficit is equal to the winding of the gauge field and that they exhibit all the properties that are expected in the continuum. It was also found in [15] that these modes are robust under the addition of high frequency noise. Using the overlap formalism, numerical simulations of the massless [17] and massive [18] vector Schwinger model gave the expected value for the anomalously generated t’Hooft vertex [17]. Furthermore, the index of the Dirac operator was calculated in SU(2) pure gauge theory slightly above the zero temperature crossover region [19]. The index agreed within one sigma with the topological

charge as calculated in [20] indicating that the index theorem holds in a statistical sense. Similar studies were done in [21] for pure SU(3) gauge theory.

The above mentioned body of work indicates that the overlap ($L_s \rightarrow \infty$ limit of domain wall fermions) successfully incorporates exact zero modes at finite and relatively large lattice spacings. This suggests that with domain wall fermions, lattice QCD describes anomalous effects with regularization artifacts under firm control. Unfortunately, a direct implementation of the overlap formalism in QCD needs computing resources that are beyond the capabilities of present day supercomputers. While a new proposal for reducing the computational cost of the overlap has been made [23], [24], it is not yet clear what the QCD computing requirement of this method will be. On the other hand, a straight-forward approach is to keep L_s finite. This method was used in [18] to simulate the dynamical two flavor Schwinger model. In that work a detailed analysis of the L_s dependence indicated that for the massive theory the $L_s = \infty$ value of the chiral condensate and of the t'Hooft vertex was already reproduced within a few percent at $L_s \approx 10$. Furthermore, the rate of approach was consistent with exponential decay with a decay rate that became faster as the continuum limit was approached. Also, for an application to quenched QCD see [25].

3 Numerical Results

These promising results indicate the important possibility of practical, chirally-consistent QCD simulations with domain wall fermions at finite L_s . In preparation for such simulations we wish to investigate to what extent the zero mode properties of the $L_s = \infty$ theory are maintained at numerically accessible values of L_s ($\sim 10 - 20$). If a much larger L_s is needed then one would not be able to exploit these important features. On the other hand, if these properties are maintained at accessible values of L_s then anomalous effects can be studied with firm control over the finite L_s artifacts.

Here we investigate this question using a classical instanton-like background [6] with prescribed winding of one unit. This is a compactified, singular-gauge instanton with origin in the center of a unit hypercube. The instanton field is cut off smoothly at some radius r_{\max} so that it is entirely contained within the lattice volume. Specifically, we begin with:

$$A_\mu(x) = -i \sum_{j=1}^3 \eta^{j\mu\nu} \lambda^j \frac{x_\nu}{x^2 + \rho(r)^2} \quad , \quad \rho(r) = \rho_0 \left(1 - \frac{r}{r_{\max}}\right) \Theta(r_{\max} - r) \quad (1)$$

where A_μ is the gauge field potential, x_ν is the space-time coordinate, r is the magnitude of x , λ^j , $j = 1, 2, 3$ are the first three Gell-Mann matrices, $\eta^{j\mu\nu}$ is as in [1], Θ is the usual Heavyside function and ρ_0 is the instanton radius. Outside the fixed radius r_{\max} the configuration is strictly a gauge transformation. This continuum field is then transcribed in the standard way to a lattice configuration of group elements, $U_\mu(x)$, defined on the lattice links x, μ . Finally, the lattice equivalent of the continuum transformation to singular gauge is applied:

$$U_\mu(x) \rightarrow g(x) U_\mu(x) g^{-1}(x + a_\mu) \quad , \quad g(x) = \sum_{j=0}^3 \frac{x_j \lambda^j}{|x|} \quad (2)$$

where λ^0 is the identity matrix and a_μ is a unit vector along the direction μ . Provided that the instanton center is not on a lattice site, this transformation is well defined everywhere. After the transformation, all links lying entirely outside r_{\max} are equal to the unit matrix so the configuration exactly obeys the usual periodic boundary conditions. This instanton field is implemented on an 8^4 lattice with $\rho_0 = 10$, $r_{\max} = 3$ and on a 16^4 lattice with $\rho_0 = 20$, $r_{\max} = 7$. Thus, upon moving from the smaller to the larger lattice, we have reduced the lattice spacing, measured in units of the instanton radius, by nearly a factor of two. In order to study the robustness of zero modes, random fluctuations with a given amplitude ζ are superimposed. In particular, at each link a different $SU(3)$ matrix is constructed by exponentiating a linear combination of Gell-Mann matrices with random coefficients in the range $[-\zeta, \zeta]$. The gauge field at each link is then multiplied by these matrices.

The operator used to study the effects of the winding of the gauge field background on the fermion sector is the chiral condensate $\langle \bar{q}q \rangle$ calculated on that background. For staggered fermions $\langle \bar{q}q \rangle = \frac{1}{3V} Tr[D^{-1}]$ where D is the standard staggered Dirac operator and V is the four-dimensional volume. For domain wall fermions $\langle \bar{q}q \rangle = \frac{1}{12V} Tr[(D^{-1})_{4d}]$ where D is the five-dimensional Dirac operator of [12], $(D^{-1})_{4d}$ is its inverse with the fifth dimension indices fixed so that it corresponds to a propagator between four-dimensional quark fields that are projections of the 5-dimensional fields as prescribed in [12], and V is the four-dimensional volume. In particular, a four-dimensional Dirac spinor field is formed by combining the two upper spin components of the five-dimensional Dirac spinor field at $s = 0$ with the lower two spin components at $s = L_s - 1$. This Dirac operator contains an explicit mass term that mixes the right and left chiralities with strength m_f . Antiperiodic boundary conditions along the time direction were implemented for both staggered and domain wall fermions. The inversion was done using the conjugate gradient algorithm. The stopping condition (ratio of the residual over the norm of the source) was set to: 10^{-5} for masses in the range $[10^{-1}, 10^{-2}]$, 10^{-6} for masses in the range $(10^{-2}, 10^{-3}]$, 10^{-7} for masses in the range $(10^{-3}, 10^{-4}]$, and 10^{-8} for masses in the range $(10^{-4}, 10^{-5}]$.

The trace is over space-time, spin and color. A stochastic estimator was used to calculate the trace. To get reasonable estimates of the average and error one would have to use a large number (~ 50) of Gaussian random vectors. However, in this paper the interest is not so much in the actual value of the trace since it is only used as a device in studying the smallest eigenvalue (topological zero mode) of the domain wall fermion Dirac operator. To the extent that the Dirac propagator which enters $\langle \bar{q}q \rangle$ is dominated by this single eigenvector of interest, the complete trace might be replaced by a single diagonal element taken in a random direction. This would give the desired trace, multiplied by the overlap between the random vector and the dominant zero mode. If the same random vector is used for all values of m_0 , m_f and L_s , it is expected that this overlap will be essentially constant and the variations seen will be those present in the full trace[6]. This strategy is followed in the calculation. However, in order to reduce the chance that the contribution of the single eigenvector of interest is accidentally suppressed by an unfortunate choice of random diagonal element, the same set of ten Gaussian random vectors is used to approximate the trace for all values of m_0 , m_f and L_s . The error bars shown in the figures represent the fluctuations seen among these ten random vectors. Given this small number of samples, it is not certain that these error estimates are accurate. However, additional calculation

suggests that this particular sample probably underestimates the errors by less than a factor of two.

At infinite L_s the explicit overlap formula for this formulation was derived in [12]. Using that it can be shown that $\langle \bar{q}q \rangle$ diverges as $\langle \bar{q}q \rangle \sim |\nu|/m_f$, where ν is the index of the Dirac operator as defined by the overlap formalism. At finite L_s the two chiralities do not completely decouple and therefore there is a residual mass. In free field theory this mass decreases exponentially with L_s and the effective quark mass is proportional to the sum of the residual mass and the explicit mass m_f . In particular [18]:

$$m_{\text{eff}} = m_0(2 - m_0)[m_f + (1 - m_0)^{L_s}] \quad (3)$$

where m_0 is the mass (domain wall height) of the five dimensional theory. In free field theory one flavor physics is obtained for m_0 in the interval $[0, 2)$ [10]. In the interacting theory the boundaries of this interval will be renormalized. Assuming a similar modification of the effective quark mass for the case of the instanton-like background one would expect that at finite L_s , $\langle \bar{q}q \rangle$ would behave as $\langle \bar{q}q \rangle \sim |\nu|/[m_f + (1 - m'_0)^{L_s}]$, where $m'_0 = m'_0(m_0)$ is a “renormalized” domain wall height.

As mentioned above, the index of the Dirac operator in the overlap formalism is naturally integer valued. A method to measure this index was developed in [15] and used in [19], [16], [21], [22]. The index is half the difference of the number N_+ of positive minus the number N_- of negative eigenvalues of the Hamiltonian H associated with the transfer matrix T . This number is the same as half the difference of the number of positive and negative eigenvalues of the operator $D = \gamma_5 D_w$ where D_w is the standard Wilson Dirac operator evaluated at a mass which is the negative of the domain wall height, *i.e.* $-m_0$ [15] [12]. For $m_0 < 0$ it can be shown that $N_+ = N_-$ for any background gauge field. Therefore, by monitoring a few of the small positive and negative eigenvalues of $D(m_0)$ as m_0 is varied between zero and the positive value of interest, one can determine the number of positive eigenvalues that crossed zero and became negative and the number of negative eigenvalues that crossed zero and became positive. The difference of the number of the two types of crossings is the index.

For the classical backgrounds that we studied we found that on the 8^4 lattice the index changed from zero to one at $m_0 \approx 0.28$ and back from one to zero at $m_0 \approx 2.14$. For the 16^4 lattice the index changed at $m_0 \approx 0.05$ and $m_0 \approx 2.01$. (Note this approach to the free-field values of 0 and 2 is expected as one goes to the smaller lattice spacing implied by our 16^4 instanton-like configuration.) These values change by less than 1% when noise was added. Therefore, in these intervals one expects $\langle \bar{q}q \rangle$ to diverge as m_{eff} is made small. At the crossing points the transfer matrix has a unit eigenvalue and even at $L_s = \infty$ the two chiralities do not decouple [15]. Therefore, near a crossing larger values of L_s may be needed to see the expected $1/m$ behavior [12].

A “sketch” of the expected behavior of $\langle \bar{q}q \rangle$ versus m_f in the presence of a gauge field background with net winding is presented in Figure 1. In order to facilitate the comparison with staggered fermions, we will also use m_f for the usual staggered fermion mass. It is useful to analyze the mass dependence of $\langle \bar{q}q \rangle$ by reference to the functional form of the spectral formula

$$\langle \bar{q}q \rangle = [m/V] \sum_{\lambda} \{1/(\lambda^2 + m^2)\}. \quad (4)$$

This continuum equation is exact for the case of staggered fermions and offers a useful framework for discussion of domain wall fermions. We can distinguish four distinct regions suggested by this functional form. In the large m_f region (I), we expect the propagator to be dominated by the mass term and therefore $\langle \bar{q}q \rangle \sim 1/m_f$. This behavior is expected and seen for both domain wall and staggered fermions. Next, we define region (III) for staggered fermions, as the mass range within which m_f is small but larger than the smallest eigenvalue λ_{\min} . Here, λ_{\min} is presumably shifted away from zero by finite lattice spacing effects. For staggered fermions λ_{\min} is four-fold degenerate or near degenerate for the case where noise has been added. Region (III) is defined similarly for domain wall fermions, except the condition $m_f \geq \lambda_{\min}$ is replaced by $m_f \geq m_{\text{res}}$, the residual mass due to the mixing of chiralities between the walls. (For the free field case, this is the $(1 - m_0)^{L_s}$ term in equation 3.) Although, domain wall fermions in the $L_s \rightarrow \infty$ limit have $\lambda_{\min} = 0$ its effects at finite L_s are cut off by this residual mass. Thus, for both staggered and domain wall fermions, one expects the small eigenvalue mode(s) to dominate the value of $\langle \bar{q}q \rangle$ in region (III) and therefore $\langle \bar{q}q \rangle \sim 1/(m_f V)$ where V is the lattice volume. Region (II) is the crossover region between region (I) and region (III). In much of this region the mass is much larger than λ_{\min} but is small enough to be relatively unimportant when compared with the rest of the eigenvalue spectrum. Therefore, referring to equation 4, one would expect $\langle \bar{q}q \rangle \sim m_f$ in much of region (II).

The expected behavior in region (IV) is different for staggered and domain wall fermions. For staggered fermions (solid line) λ_{\min} is small but not zero. Thus, in region (IV), where $m_f < \lambda_{\min}$, the effects of the factor of m_f in the numerator of eq. 4 will dominate and therefore one would expect $\langle \bar{q}q \rangle \sim m_f$. In contrast, for domain wall fermions (dashed line) and $m_f < m_{\text{res}}$, we expect m_{res} to play the role of m in eq. 4 so that in region (IV) $\langle \bar{q}q \rangle \approx \text{const}$. For domain wall fermions, region (IV) is dominated by the finite L_s , residual mixing of the two four-dimensional boundaries (see eq. 3). In the numerical results of this paper region (I) and part of region (II) are not present because the largest mass is $m_f = 10^{-1}$. The focus is on region (III) where the divergent $1/m_f$ behavior is expected and on the beginning of region (IV) whose onset signals the need for larger values of L_s .

The numerical results are presented in Figures 2 – 8. In Figure 2 the staggered $\langle \bar{q}q \rangle$ is plotted versus the quark mass m_f in the presence of the compactified, singular-gauge instanton background. Two lattice volumes and three different noise amplitudes, $\zeta = 0, 0.01, 0.1$, are shown. For the case of the 8^4 lattice with no noise, one may be able to recognize divergent, $1/m_f$ behavior in $\langle \bar{q}q \rangle$ for $10^{-2} \leq m_f \leq 10^{-1}$ indicating the presence of a near-zero mode. This divergent behavior does not extend to smaller m_f presumably because of the zero mode shift effect [5]. As can be seen when the lattice size is increased from 8^4 to 16^4 the instanton field becomes “smoother” (lattice spacing is reduced by a factor of two) and the divergent behavior becomes more pronounced now extending to the region $10^{-4} \leq m_f \leq 10^{-2}$. For a detailed analysis the reader is referred to [6]. However, when noise is added the divergent behavior begins to disappear. At noise amplitudes of 0.1 the divergent behavior is not present in the 8^4 lattice while in the 16^4 lattice it has been significantly reduced.

Figure 3 is the same as Figure 2 but now for the domain wall fermion $\langle \bar{q}q \rangle$ with $m_0 = 1.2$. Results are shown for the two volumes 8^4 and 16^4 and for $L_s = 4, 6, 8, 10$. As can be seen, $\langle \bar{q}q \rangle \sim 1/m_f$ for small m_f . As expected, when m_f becomes smaller than some value, the

residual mixing between the two chiralities becomes the dominant contribution to m_{eff} and $\langle \bar{q}q \rangle$ stops changing. This value is the border between regions (IV) and (III) sketched in Figure 1. For the 16^4 lattice and for $L_s = 6, 8, 10$ one finds that $\langle \bar{q}q \rangle \sim 1/m_f$ for m_f as small as $\approx 10^{-5}$. For $L_s = 4$ there is no signal of a divergence because the effective quark mass is dominated by the finite L_s residual mass. For the 8^4 lattice similar behavior is observed but now for $L_s = 8, 10$. For $L_s = 6$ a divergence is observed but only for m_f down to $\approx 10^{-3}$. When noise is added with amplitudes $\zeta = 0.01$ and $\zeta = 0.1$ the behavior remains unaffected for all practical purposes indicating robustness under high frequency noise. For $\zeta = 1$ the zero modes disappear (not shown here) but this level of noise is so large that it presumably destroys the winding. In particular, the index of the Dirac operator, as defined by the overlap formalism, was found to be zero.

In Figure 4 the 16^4 lattice of Figure 3 for $\zeta = 0.1$ and $L_s = 10$ is plotted again, this time with a $\langle \bar{q}q \rangle = c_{-1}/m_f$ fit for $10^{-5} \leq m_f \leq 10^{-3}$ superimposed. The coefficient c_{-1} is $1.09(7) \times 10^{-6}$ and the χ^2 per degree of freedom is ≈ 0.5 , demonstrating quantitatively the expected m_f^{-1} behavior.

In order to study the m_0 dependence, $\langle \bar{q}q \rangle$ versus m_0 is plotted in Figure 5 for fixed $m_f = 5 \times 10^{-4}$. The vertical lines indicate the values of m_0 where $\gamma_5 D_w(m_0)$ has a crossing. One can see that near the crossing points larger values of L_s are required before $\langle \bar{q}q \rangle$ becomes independent of L_s . However, there is a large range of m_0 in between the crossings for which $\langle \bar{q}q \rangle$ does not change much when L_s is changed from 8 to 10. This means that no fine tuning of m_0 is needed even when large amounts of ultraviolet noise are added. The shape of the curves can be attributed to the wave function normalization factor which is a function of m_0 . In the free theory this factor is $m_0(2 - m_0)$ [18].

To further verify robustness under changes of m_0 , $\langle \bar{q}q \rangle$ versus m_f is studied for $m_0 = 0.75$. As can be seen from Figure 5 this value of m_0 is in the onset of the region where the L_s dependence becomes stronger. The results for $L_s = 4, 6, 8, 10, 12$ are presented in Figure 6. Also, $L_s = 24$ is presented for the 8^4 lattice. As can be seen, the zero mode effects are maintained and are robust under high frequency noise but larger L_s is needed before $\langle \bar{q}q \rangle$ becomes independent of L_s . For the 16^4 lattice $\langle \bar{q}q \rangle$ becomes independent of L_s for $L_s = 12$, but for the 8^4 lattice this does not happen until $L_s = 24$. This is expected since the crossing point for the 8^4 lattice is closer to $m_0 = 0.75$ than the crossing point for the 16^4 lattice.

If m_0 is allowed to get close to the crossing point one would expect that in order to maintain the zero mode effects much larger values of L_s may be needed. Figure 7 is the same as Figure 6, except that here m_0 is chosen a fixed distance of 0.2 from the crossing point. For the 8^4 lattice $m_0 = 0.5$ and for the 16^4 lattice $m_0 = 0.25$. The plots for $L_s = 8, 12, 16$ and 24 are shown. Also for the 8^4 lattice the plot for $L_s = 48$ is presented. As can be seen for both volumes $L_s = 24$ is barely adequate to maintain the zero mode effect for masses $5 \times 10^{-3} < m_f$. In order to maintain zero mode effects for masses $10^{-4} < m_f < 5 \times 10^{-3}$ an $L_s = 48$ is needed for the 8^4 lattice.

Finally, $\langle \bar{q}q \rangle$ is plotted versus L_s in figure 8 for zero noise amplitude, fixed $m_f = 5 \times 10^{-4}$ and for three values of $m_0 = 0.5, 0.75$ and 1.2 corresponding to circles, squares and crosses. The fits are to a function of the form $1/[c_0 + c_1 e^{-c_2 L_s}]$. For the three values of m_0 the fitting range of L_s is $[8, 48]$, $[6, 48]$ and $[4, 48]$, the coefficient $c_0 = 0.183(8), 0.44(3)$ and $0.91(31)$, and the χ^2/dof is 4×10^{-2} , 4×10^{-2} and 2×10^{-4} . (Note, these fits were performed by

minimizing the simplest χ^2 , which did not incorporate the strong correlation between the fluctuations at different values of L_s . The presence of such correlations, resulting from using the same random source vectors for each L_s , is reflected in the abnormally small values of χ^2 .) Again, the quality of these fits demonstrates the expected $1/m_{\text{eff}} \sim 1/[m_f + m_{\text{res}}]$ dependence of $\langle \bar{q}q \rangle$ but this time m_f is held fixed while $m_{\text{res}} \sim e^{-c_2 L_s}$ is varied. As expected, the decay rate is fast for $m_0 = 1.2$ but as m_0 gets closer to the value where $\gamma_5 D_w$ has a crossing the decay rate becomes slower. Also, as expected from the discussion relating to equation 4 and figure 1 when m_{res} becomes large the behavior changes from the monotonic behavior of regions IV and III to that of region II. For $m_0 = 0.5$ this can be seen for $L_s = 4, 6$ and for $m_0 = 0.75$ it can be seen for $L_s = 4$. For $m_0 = 1.2$ presumably m_{res} does not get large even for $L_s = 4$ and there is no change in the monotonic behavior.

4 Conclusions

In conclusion, for a classical, instanton-like background the domain wall fermion chiral condensate diverges as $\langle \bar{q}q \rangle \sim 1/m_f$ for m_f as small as 10^{-5} and L_s as small as ~ 10 lattice spacings. This behavior was observed on lattices of size 8^4 and 16^4 and was robust under random, high frequency noise with amplitudes as large as $\zeta = 0.1$. This $1/m_f$ divergence was observed for a wide range of values of m_0 , indicating that there is no need for a fine tuning of m_0 . Furthermore, at fixed m_f and m_0 the chiral condensate approaches its $L_s = \infty$ asymptotic value exponentially fast with a rate that becomes faster as m_0 is varied away from the point where the index of the Dirac operator changes. Therefore, domain wall fermions continue to show their spectacular $L_s = \infty$ zero-mode properties even for values of m_f and L_s that are practically accessible to contemporary numerical simulations. Numerical simulations of QCD are currently under way [26] to study the zero mode effects of domain wall fermions on gauge field backgrounds with realistic quantum fluctuations.

Acknowledgments

The numerical calculations were done on the 400 Gflop QCDSF computer at Columbia University. We would like to thank R. Edwards and R. Narayanan for helpful discussions. This research was supported in part by the DOE under grant # DE-FG02-92ER40699.

References

- [1] G. 't Hooft, Phys. Rev. Lett **37** (1976) 8; Phys. Rev. **D14** (1976) 3432; Phys. Reports **142** (1986) 357.
- [2] E. Witten, Nucl. Phys. **B156** (1979) 269; G. Veneziano, Nucl. Phys. **B159** (1979) 213.
- [3] R. Pizarski and F. Wilczek, Phys. Rev. **D29** (1984) 338.
- [4] M. Atiyah, I. Singer, Ann. Math. **87** (1968) 484; L. Brown, R. Carlitz, and C. Lee, Phys. Rev. **D16** (1977) 417.

- [5] J. Smit, J. Vink, Nucl. Phys. **B286** (1987) 485; J. Vink, Nucl. Phys. **B307** (1988) 549; J. Smit, J. Vink, Nucl. Phys. **B303** (1988) 36; J. Smit, J. Vink, Phys. Lett. **B194** (1987) 433; J. Vink, Phys. Lett. **B212** (1988) 483.
- [6] A. Kaehler, in preparation.
- [7] For a recent review, see A. Ukawa, Nucl. Phys. **B53** (Proc. Suppl.) (1997) 106.
- [8] S. Chandrasekharan, D. Chen, N.H. Christ, W. Lee, R. Mawhinney, and P.M. Vranas, CU-TP-902, hep-lat 9807018.
- [9] J.B. Kogut, J.F. Lagae, D. K. Sinclair, hep-lat/9801020.
- [10] D.B. Kaplan, Phys. Lett. **B288** (1992) 342; Nucl. Phys. **B30** (Proc. Suppl.) (1993) 597.
- [11] Y. Shamir, Nucl. Phys. **B406** (1993) 90.
- [12] V. Furman, Y. Shamir, Nucl. Phys. **B439** (1995) 54.
- [13] D. Boyanovsky, E. Dagatto and E. Fradkin, Nucl. Phys. **B285** (1987) 340.
- [14] R. Narayanan, Nucl. Phys. **B34** (Proc. Suppl.) (1994) 95; M. Creutz, Nucl. Phys. **B42** (Proc. Suppl.) (1995) 56; Y. Shamir, Nucl. Phys. **B47** (Proc. Suppl.) (1996) 212.
- [15] R. Narayanan, H. Neuberger, Phys. Lett. **B302** (1993) 62; Phys. Rev. Lett. **71** (1993) 3251; Nucl. Phys. **B412** (1994) 574; Nucl. Phys. **B443** (1995) 305.
- [16] R.G. Edwards, U.M. Heller and R. Narayanan hep-lat/9801015.
- [17] R. Narayanan, H. Neuberger and P. Vranas, Phys. Lett. **B353** (1995) 507; Nucl. Phys. **B 47** (Proc. Suppl.) (1996) 596.
- [18] P.M. Vranas, Nucl. Phys. **B53** (Proc. Suppl.) (1997) 278; P.M. Vranas Phys. Rev. **D57** (1998) 1415.
- [19] R. Narayanan and P. Vranas, Nucl. Phys. **B506** (1997) 373.
- [20] Ph. de Forcrand, M. García Pérez and I.-O. Stamatescu, Nucl. Phys. **B499** (1997) 409.
- [21] R.G. Edwards, U.M. Heller and R. Narayanan hep-lat/9802016.
- [22] R.G. Edwards, U.M. Heller and R. Narayanan hep-lat/9806011.
- [23] H. Neuberger Phys. Lett. **B417** (1998) 141; Phys. Rev. **D57** (1998) 5417; RU-98-03, hep-lat/9801031; RU-98-28, hep-lat/9806025.
- [24] R.G. Edwards, U.M. Heller and R. Narayanan hep-lat/9807017.
- [25] T. Blum and A. Soni, Phys. Rev. **D56** (1997) 174; Phys. Rev. Lett. **79** (1997) 3595.

- [26] Columbia lattice group contributions to the RIKEN-BNL workshop on Fermion Frontiers on Vector Lattice Gauge Theory held May 6-9, 1998, at the Brookhaven National Laboratory;

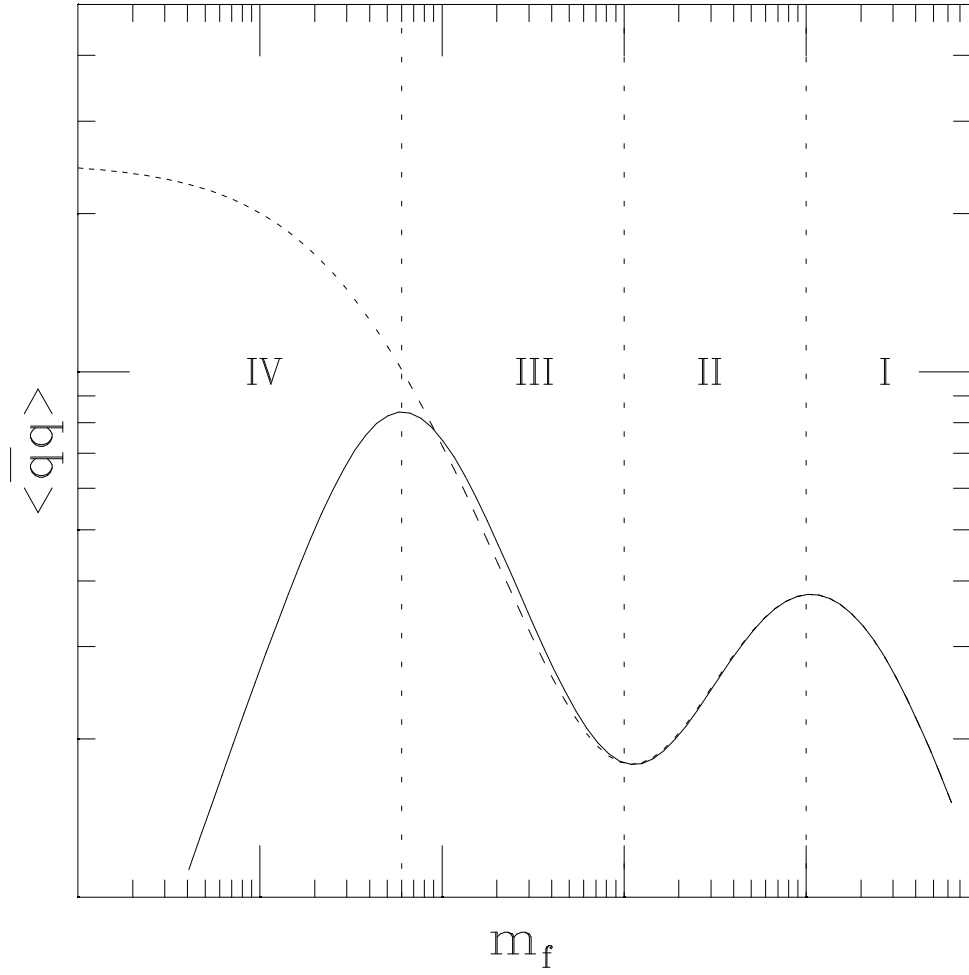


Figure 1. The expected functional form of $\langle \bar{q}q \rangle$ vs. m_f . The solid line corresponds to staggered fermions and the dashed line to domain wall fermions.

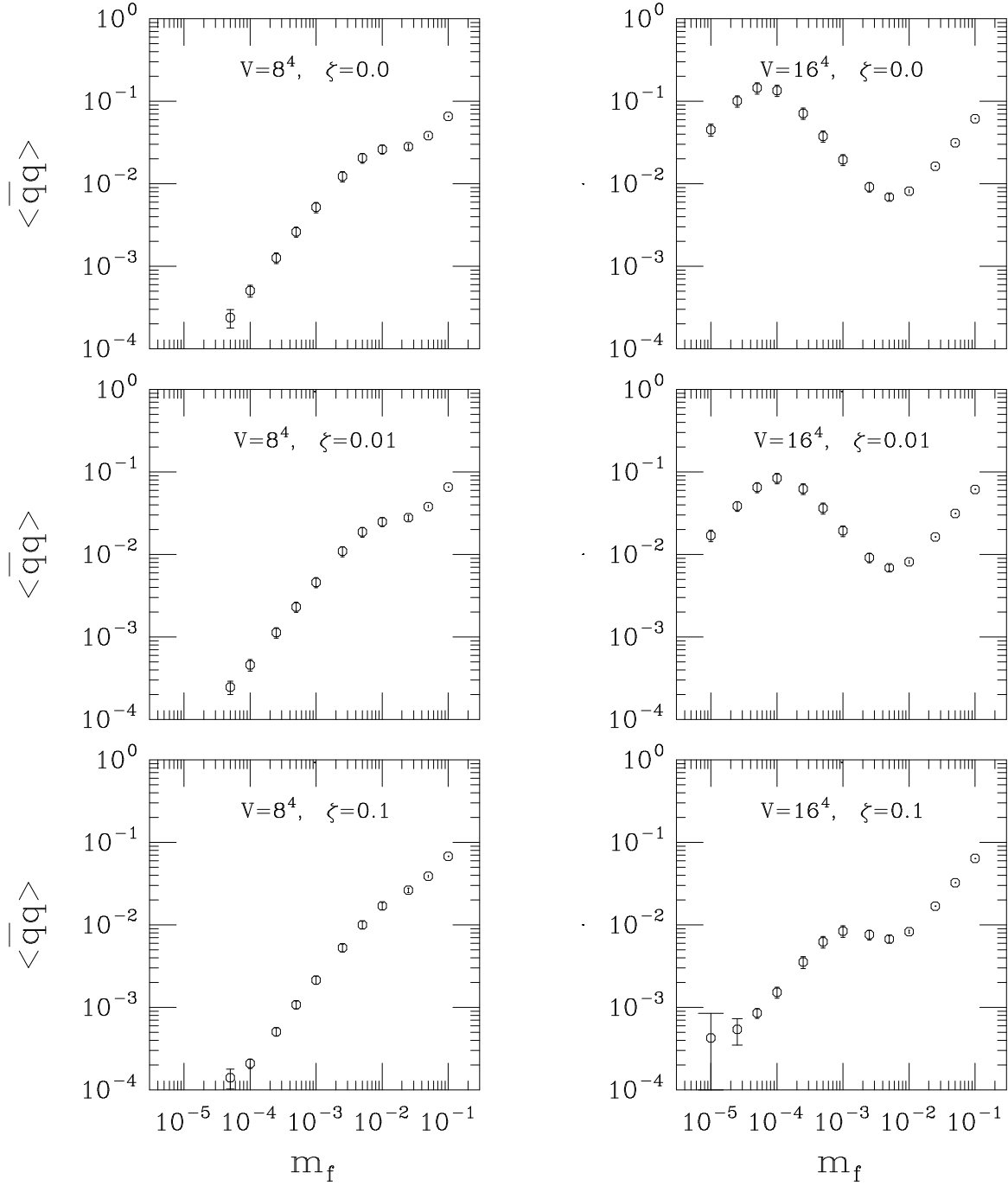


Figure 2. $\langle \bar{q}q \rangle$ vs. m_f for staggered fermions. The left columns are for an 8^4 volume and the right columns for a 16^4 volume. The $\zeta = 0$ figures correspond to the compactified singular-gauge instanton background. The $\zeta = 0.01, 0.1$ figures correspond to the same background but random noise has been superimposed with amplitude ζ .

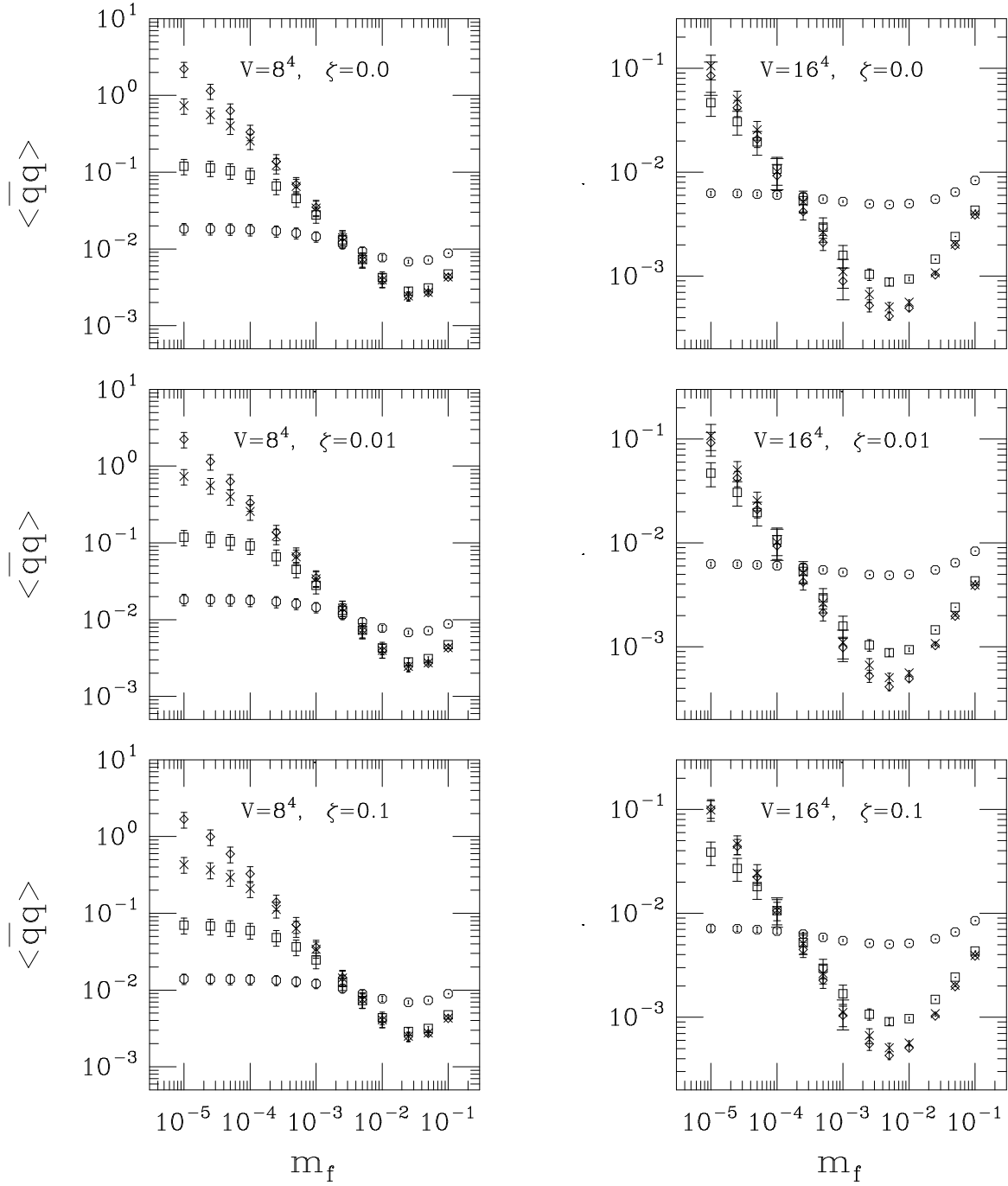


Figure 3. Same as Figure 2 but for domain wall fermions at $m_0 = 1.2$. Four different values of L_s are shown with the circles, squares, crosses, and diamonds corresponding to $L_s = 4, 6, 8, 10$.

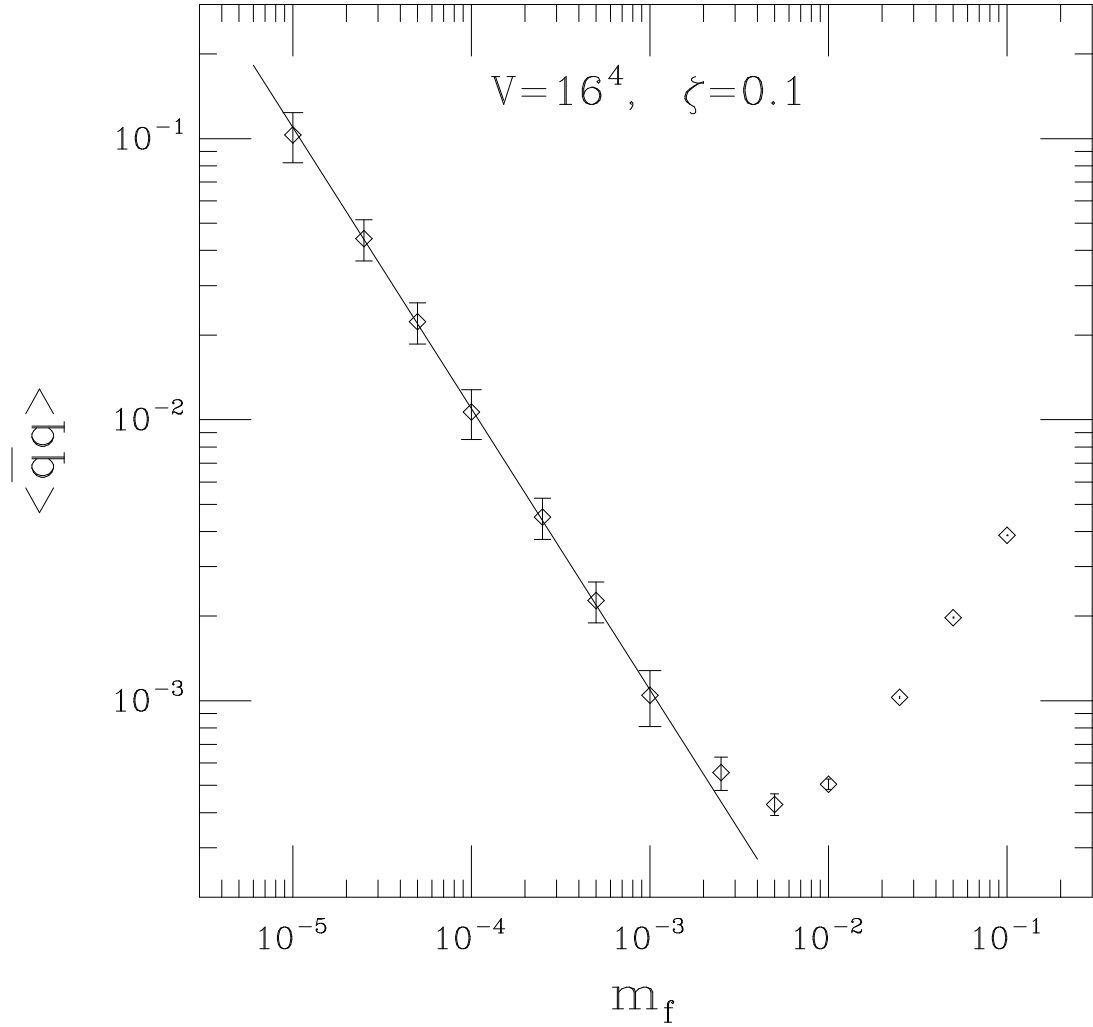


Figure 4. Same as the 16^4 lattice, $L_s = 10$, $\zeta = 0.1$ plot of Figure 3. The solid line is a fit to c_{-1}/m_f for $10^{-5} \leq m_f \leq 10^{-3}$. The fit has a χ^2 per degree of freedom ≈ 0.5 .

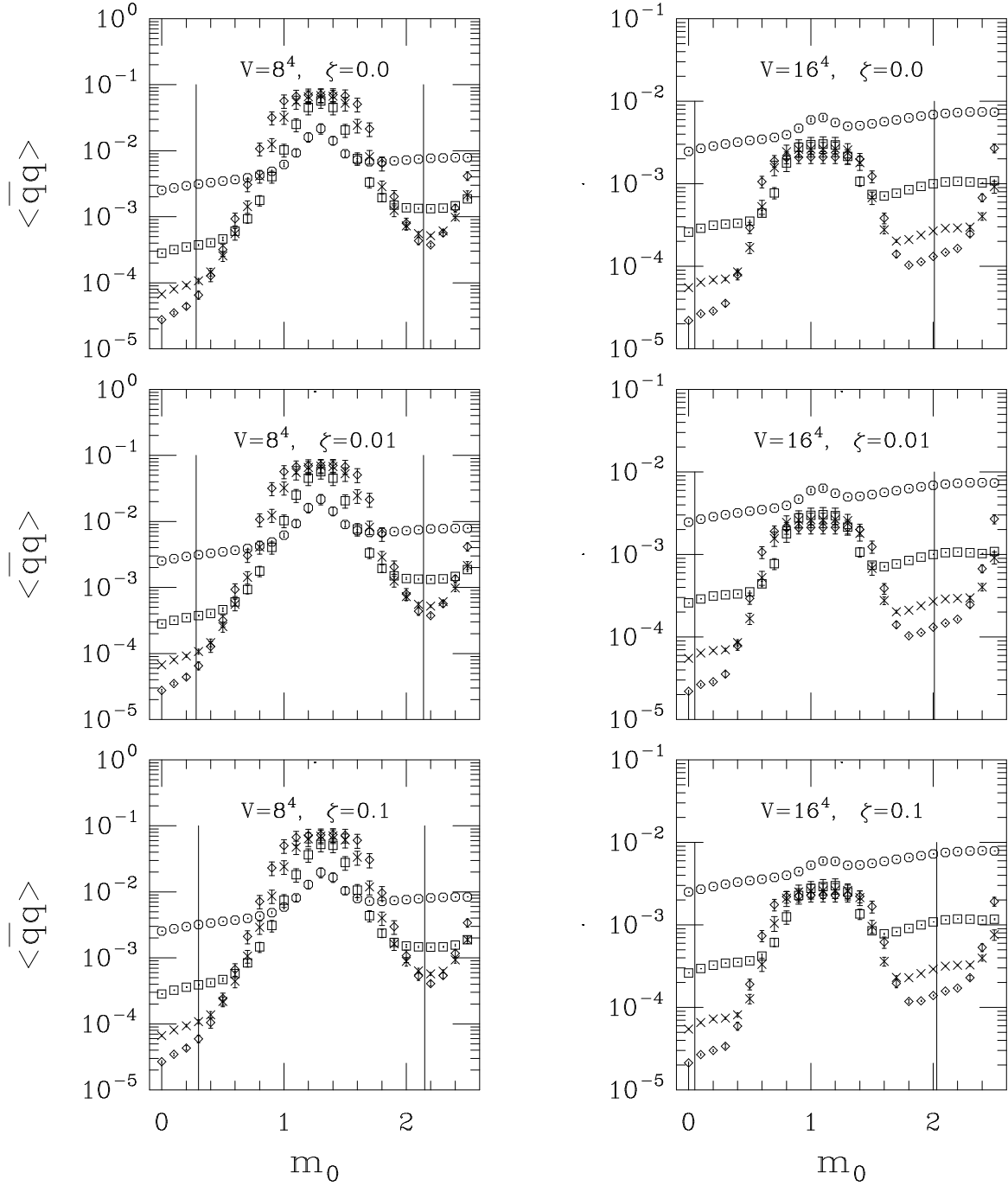


Figure 5. Same as Figure 3 but now vs. m_0 at fixed $m_f = 5 \times 10^{-4}$. The index of the Dirac operator changes at the vertical lines from zero to one and then back from one to zero. Four different values of L_s are shown with the circles, squares, crosses, and diamonds corresponding to $L_s = 4, 6, 8, 10$.

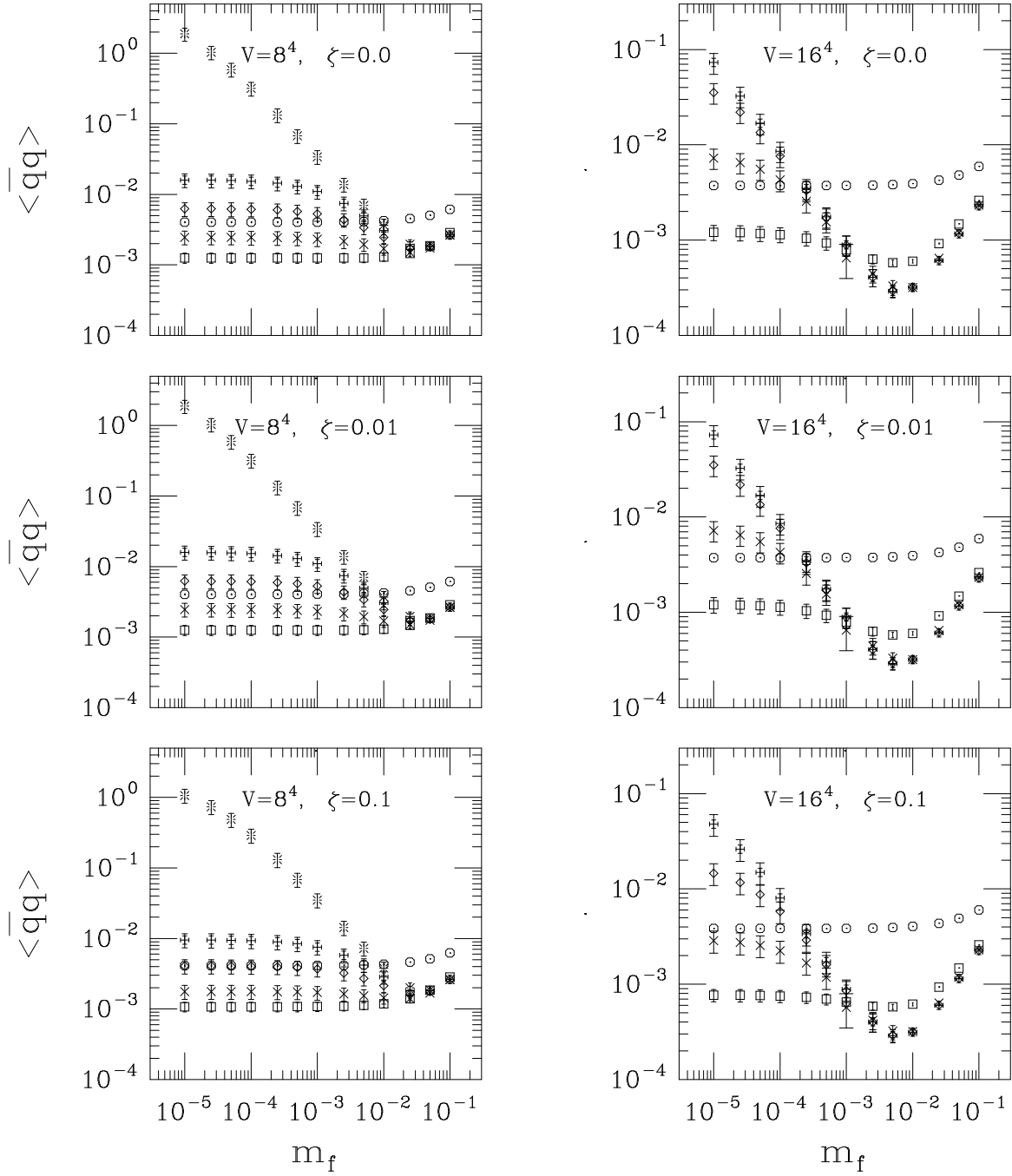


Figure 6. Same as Figure 3 but for $m_0 = 0.75$. The circles, squares, crosses, diamonds and plus symbols correspond to $L_s = 4, 6, 8, 10, 12$ respectively. The star symbols on the 8^4 graph correspond to $L_s = 24$.

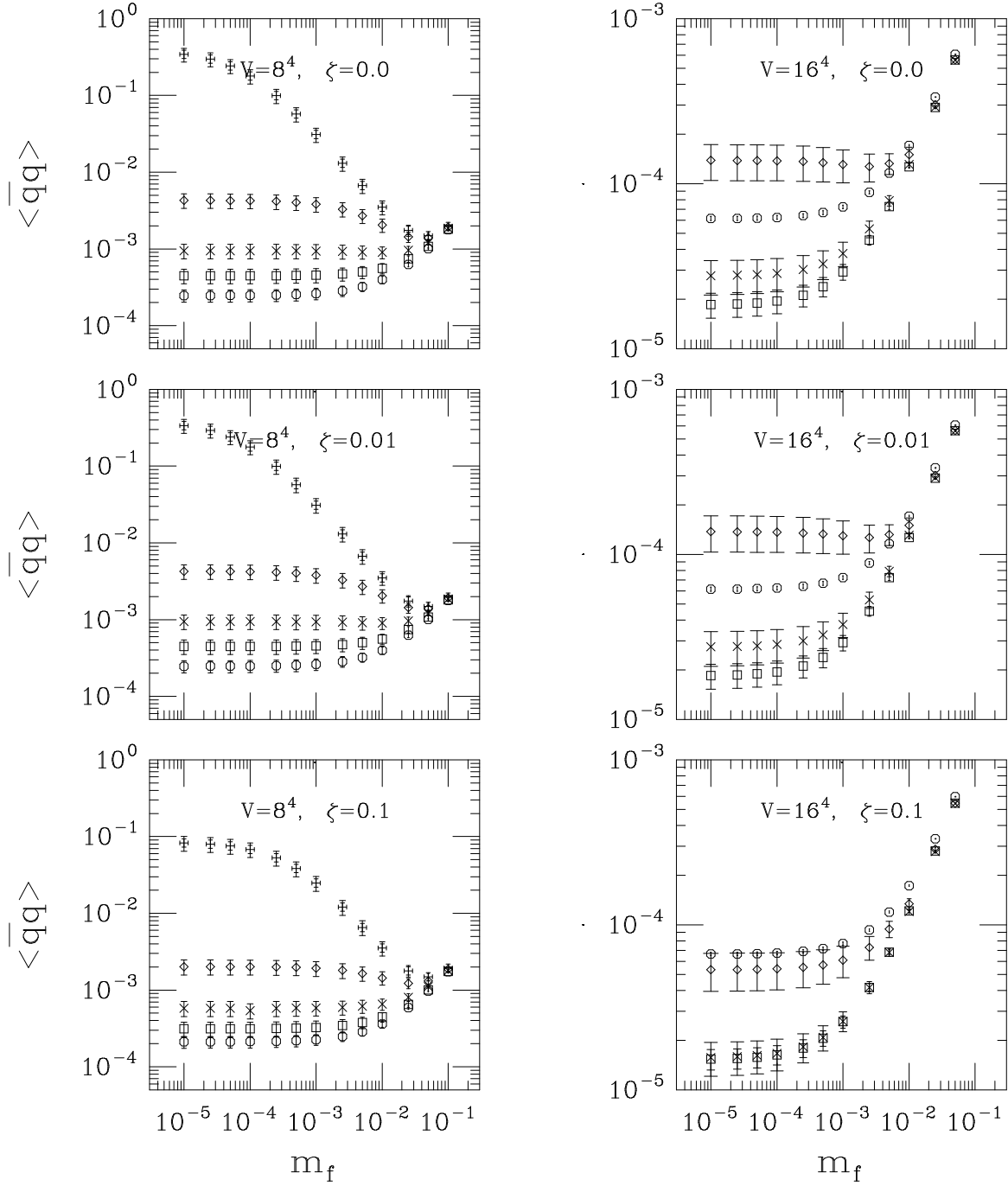


Figure 7. Same as Figure 6 but for $m_0 = 0.5$ for the 8^4 and $m_0 = 0.25$ for the 16^4 . The circles, squares, crosses and diamond symbols correspond to $L_s = 8, 12, 16, 24$ respectively. The plus symbols on the 8^4 graph correspond to $L_s = 48$.

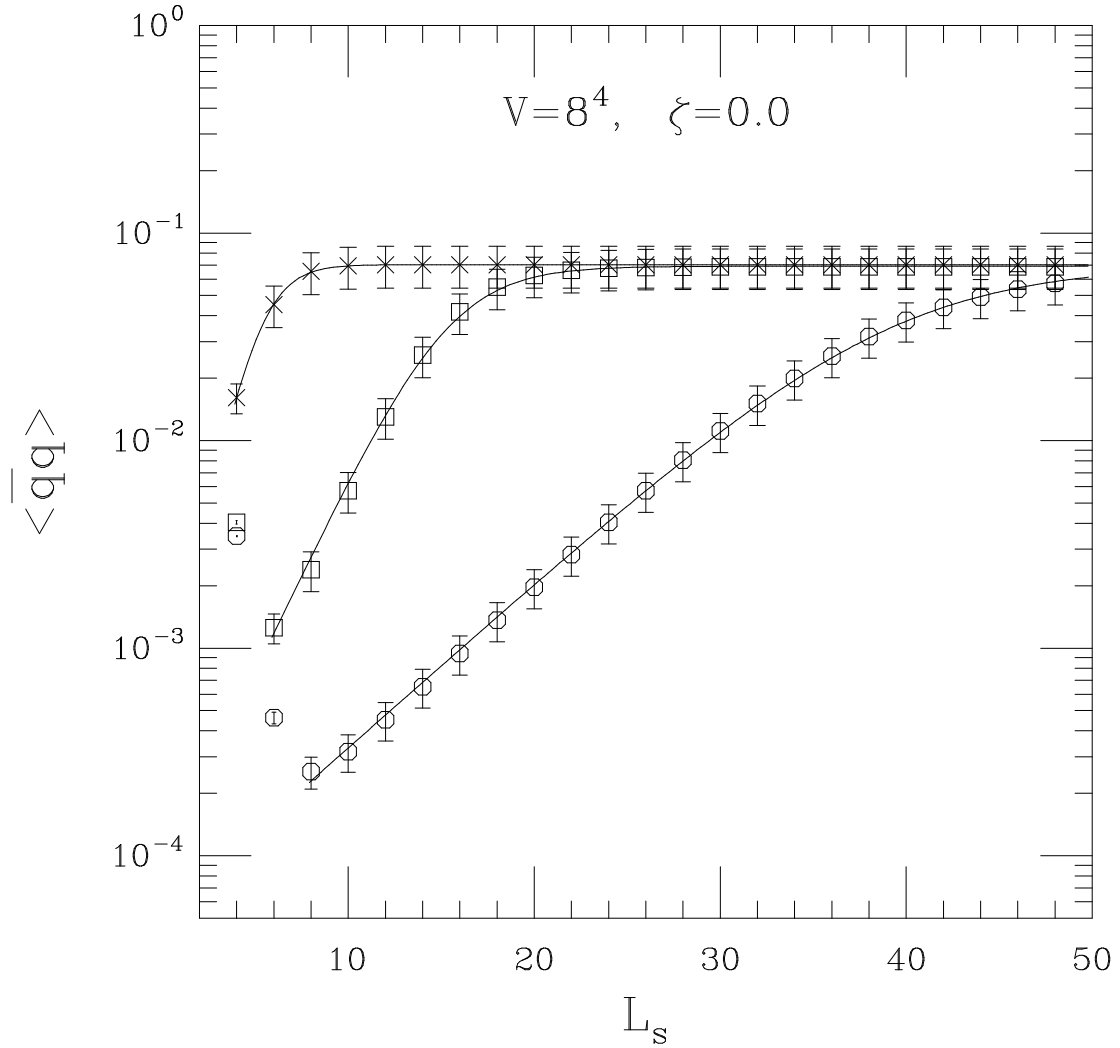


Figure 8. $\langle \bar{q}q \rangle$ vs. L_s for zero noise amplitude, fixed $m_f = 5 \times 10^{-4}$ and for three values of $m_0 = 0.5, 0.75$ and 1.2 corresponding to circles, squares and crosses. The fits are to a function of the form $1/[c_0 + c_1 e^{-c_2 L_s}]$. For the three values of m_0 the fitting range of L_s is $[8, 48]$, $[6, 48]$ and $[4, 48]$, the coefficient $c_0 = 0.183(8), 0.44(3)$ and $0.91(31)$, and the χ^2/dof is 4×10^{-2} , 4×10^{-2} and 2×10^{-4} .